Structure-exploiting Delay-dependent Stability Analysis Applied to Power System Load Frequency Control

Chao Duan, *Student Member, IEEE*, Chuan-Ke Zhang, *Member, IEEE*, Lin Jiang, *Member, IEEE*, Wanliang Fang, Wei Yao, *Member, IEEE*

***Abstract*—Linear matrix inequality (LMI) based delay-dependent stability analysis/synthesis methods have been applied to power system load frequency control (LFC) which has communication networks in its loops. However, the computational burden of solving large-scale LMIs poses a great challenge to the application of those methods to real-world power systems. This paper investigates the computational aspect of delay-dependent stability analysis (DDSA) of LFC. The basic idea is to improve the numerical tractability of DDSA by exploiting the chordal sparsity and symmetry of the graph related to LFC loops. The graph-theoretic analysis yields the structure restrictions of weighting matrices needed for the LMIs to inherit the chordal sparsity of the control loops. By enforcing those structure restrictions on weighting matrices, the positive semi-definite constraints in the LMIs can be decomposed into smaller ones, and the number of decision variables can be greatly reduced. Symmetry in LFC control loops is also exploited to reduce the number of decision variables. Numerical studies show the proposed structure-exploiting techniques significantly improves the numerical tractability of DDSA at the cost of the introduction of acceptable minor conservatism.**

***Index Terms*—Delay-dependent stability, load frequency control, chordal sparsity, symmetry, linear matrix inequality.**

I. Introduction

The existence and adverse effects of time delays in power system control loops have been well-recognised by recent publications with the ever-increasing integration of communication networks into the closed-loop control & operation of the currently developing smart grids. Time delays can degrade the dynamic performance and stability of load frequency control (LFC) [1]–[5]. To analyze and further alleviate the effects of time delays, many researchers have focused their attention on delay margin calculation and time-delay robust control.

Delay margins are the maximal admissible time delays with which the system remains stable [2], [4]. The knowledge of the delay margins can be used to evaluate the stability level and guide the controller design of time-delay power systems. Two groups of methods, including frequency-domain and time-domain methods, have been proposed to calculate the delay margins. Frequency-domain methods obtain the delay margins by computing all critical roots of system characteristic equations [6], [7]. This group of methods are also successfully applied to time-delay power systems [5], [8]–[12]. Although frequency-domain methods can obtain exact delay margins, they are limited to constant delays which rarely occur in practice. Time-domain methods establish sufficient conditions for the stability of time-delay systems by constructing Lyapunov-Krasovskii functionals (LKF) whose parameters can be determined by solving linear matrix inequalities (LMI) [13]. This group of methods are applied to LFC with constant and time-varying delays [2], [4]. LMI-based time domain methods can even be extended to analyze the stability of nonlinearly perturbed LFC with time delays [14]. Although time-domain methods possess some conservatism when calculating the delay margins, they can be conveniently applied to systems with single or multiple, constant or time-varying delays. Moreover, the development of the modern interior point method (IPM) provides off-the-shelf tools to solve LMIs.

The ultimate goal of DDSA is to inform the controller design to mitigate the adverse effects of time delays. From this aspect, time-domain LMI based methods have advantages over frequency domain methods due to the fact that LMI based criteria can be conveniently employed to derive the delay-independent and delay-dependent bounded real lemmas (BRL) [13] which then can be used to design H_∞ robust controllers. For instance, delay-independent BRLs are used in [1] and [15] to design state-feedback and PI robust controllers for LFC, respectively. In [3], PID-type robust controllers are designed for LFC systems based on a delay-dependent BRL. The delay-dependent BRL in [16] is extended to consider LFC parameter uncertainties. To reduce conservatism, some probabilistic information of time delays are taken into account in the delay-dependent BRL for robust LFC design in [17]. Above-mentioned controllers are all designed to minimize the H_∞ index while guarantee stability for any delays less than the preset upper bounds (the upper bounds are ∞ for delay-independent methods).

Manuscript received June 22, 2015; revised October 24, 2016 and January 02, 2017; accepted February 10, 2017. This work was supported in part by National Natural Science Foundation of China (No. 51428702), Engineering and Physical Sciences Research Council (EP/L014351/1), National Key Research and Development Program of China (2016YFB0901903), and National Natural Science Foundation of China (No. 61503351). *(Corresponding author: C.K. Zhang.)*

C. Duan and W. Fang are with the Department of Electrical Engineering, Xi'an Jiaotong University, Xi'an 710049, China. C. Duan is also with the Department of Electrical Engineering and Electronics, University of Liverpool, Liverpool L69 3GJ, U.K. (e-mail: duanchao@stu.xjtu.edu.cn; eewlfang@mail.xjtu.edu.cn)

C.K. Zhang is with the School of Automation, China University of Geosciences, Wuhan 430074, China, with Hubei key Laboratory of Advanced Control and Intelligent Automation for Complex Systems, Wuhan 430074, China, and also with the Department of Electrical Engineering & Electronics, University of Liverpool, Liverpool L69 3GJ, U.K. (e-mail: ckzhang@cug.edu.cn)

L. Jiang is with the Department of Electrical Engineering & Electronics, University of Liverpool, Liverpool L69 3GJ, U.K. (e-mail: ljiang@liverpool.ac.uk)

W. Yao is with the State Key Laboratory of Advanced Electromagnetic Engineering and Technology, Huazhong University of Science and Technology, Wuhan 430074, China. (e-mail: w.yao@hust.edu.cn)

However, there is still a long way to go before all those analysis/synthesis methods for time-delay systems can be applied to real-world power systems. The major obstacle for time-domain LMI based methods is the computational burden of solving large-scale LMIs. Due to the limited ability of the state-of-art LMI solvers, LMI based methods are only applied to power systems with less than 3 generation units in each control area [2]–[4] or using order-reduced system models [18], [19]. As we know, there could be hundreds of generation units in a practical power system and the analysis based on order-reduced system models may not obtain reliable results. Therefore, this paper focuses on the computational aspect and aims at improving the numerical tractability of LMI based DDSA. All previous works in this field directly apply certain methods to LFC without considering the specific structure of power system control loops. Nevertheless, problems appear in the power systems are not generic ones but rather present some structures. Thus, if those structures are properly exploited, more efficient and feasible computational methods can be obtained.

The contribution of this paper is exploiting the structures, including chordal sparsity and symmetry, of LFC loops to significantly improve the numerical tractability of DDSA. The idea of exploiting chordal sparsity in Lyapunov LMI has already been discussed in [20]. We further extend this idea to DDSA by proving some more general results concerning the structure restrictions of weighting matrices needed for the LMIs in DDSA to inherit the chordal sparsity of LFC loops. Chordal sparsity in the LMIs then allows the decomposition of the original positive semi-definite (PSD) condition into much smaller ones. Moreover, the symmetry of LFC control loops is exploited to reduce the number of decision variables. By exploiting chordal sparsity and symmetry, the number of decision variables and size of PSD conditions are greatly reduced. Numerical results show the proposed structure-exploiting techniques significantly improves the numerical tractability of DDSA applied to large-scale LFC problems at the price of introducing minor and acceptable conservatism.

The rest of this paper is organized as follows. Section II describes the structure of time-delay LFC systems and the delay-dependent stability criterion. In section III, we present the chordal-structure matrix decomposition (CSMD) and give several lemmas which enable the application of CSMD to DDSA. Section IV introduces the sparsity and symmetry exploiting techniques in DDSA of LFC. Step-by-step implementation guideline is also given in this section. Section V reports numerical studies. Possible extensions of the proposed method is discussed in section VI. Finally, section VII draws conclusions and gives suggestions on future research.

II. Time-delay Load Frequency Control and Delay-dependent Stability Analysis

A. Load Frequency Control Loops

As the main function of automatic generation control (AGC) system, LFC aims at maintaining frequency and power interchanges between neighboring control areas at scheduled values [15]. Both the single-area and multi-area control schemes are shown in Fig. 1. The modeling of LFC system is mainly based on two simplifications [15], [21]: 1) LFC focuses on the collective performance of all generators rather than the inter-machine oscillations, therefore all generators in one control area are aggregated into one generator with inertia M_i equal to the sum of the inertia of all generators and the damping effect of all loads is represented by a single damping constant D_i; 2) due to the first simplification and the slow dynamics of prime-mover power change and system frequency response, the dynamics of electrical angle voltages are all neglected. As a result, the LFC model consists of governor, turbine and rotor/load, and a PI controller is implemented in practice to guarantee system stability and desirable dynamic performance. The time delays, including communication delays, sample-induced delays and fault-induced delays, are combined as one delay in the control loop represented by the block $e^{-s\tau_i}$. The formulation of the state-space model can be found in appendix A. The control loops are naturally associated with a graph representing the connection relationship among state variables, shown in Fig. 2. In this paper, we will exploit the structure characteristics of this graph, including chordal sparsity and symmetry, to improve the numerical tractability of DDSA of LFC.

B. Delay-dependent Stability Criterion

The major objectives of DDSA are to 1) calculate the system delay margins; 2) guide the controller design using the delay margins as an additional performance index. One of the mainstream methods of DDSA is based on Lyapunov-Krasovskii functionals (LKF) [13] whose existence implies the stability of time-delay systems. By specifying the structure of LKFs, sufficient conditions for stability of time-delay systems can be written as LMIs. This paper will explain the structure-exploiting techniques based on the stability criterion derived from the results in [22].

Consider the linear system with a time-varying delay:

$$\begin{cases} \dot{x}(t) = \boldsymbol{A}x(t) + \boldsymbol{A}_d x(t - d(t)),\ t > 0 \\ x(t) = \phi(t),\ t \in [-\tau, 0] \end{cases} \tag{1}$$

where $x(t) \in \mathbb{R}^n$ is the state vector; $\boldsymbol{A}$ and $\boldsymbol{A}_d$ are system matrices with appropriate dimensions; the time-varying delay $d(t)$ is a continuous function satisfying $0 \leq d(t) \leq \tau$ and $|\dot{d}(t)| \leq \mu$; the initial condition $\phi(t)$ is a continuously differentiable function on $[-\tau, 0]$. By selecting the candidate LKF as

$$\begin{aligned} v(t) = x^T(t)\boldsymbol{P}x(t) + \int_{t-d(t)}^{t} x^T(s)\boldsymbol{Q}_1 x(s)ds + \\ \int_{t-\tau}^{t} x^T(s)\boldsymbol{Q}_2 x(s)ds + \tau \int_{-\tau}^{0}\int_{t+\theta}^{t} \dot{x}^T(s)\boldsymbol{R}\dot{x}(s)dsd\theta, \end{aligned} \tag{2}$$

the following theorem certifies the stability of system (1):

Theorem 1: System (1) is asymptotically stable if there exist symmetric positive-definite matrices $\boldsymbol{P} \succ \boldsymbol{0}$, $\boldsymbol{Q}_1 \succ \boldsymbol{0}$, $\boldsymbol{Q}_2 \succ \boldsymbol{0}$, $\boldsymbol{R} \succ \boldsymbol{0}$ and a appropriately dimensioned matrix $\boldsymbol{S}$ such that

$$\boldsymbol{\Psi} = \begin{bmatrix} \boldsymbol{R} & \boldsymbol{S} \\ \boldsymbol{S}^\top & \boldsymbol{R} \end{bmatrix} \succcurlyeq \boldsymbol{0} \tag{3}$$

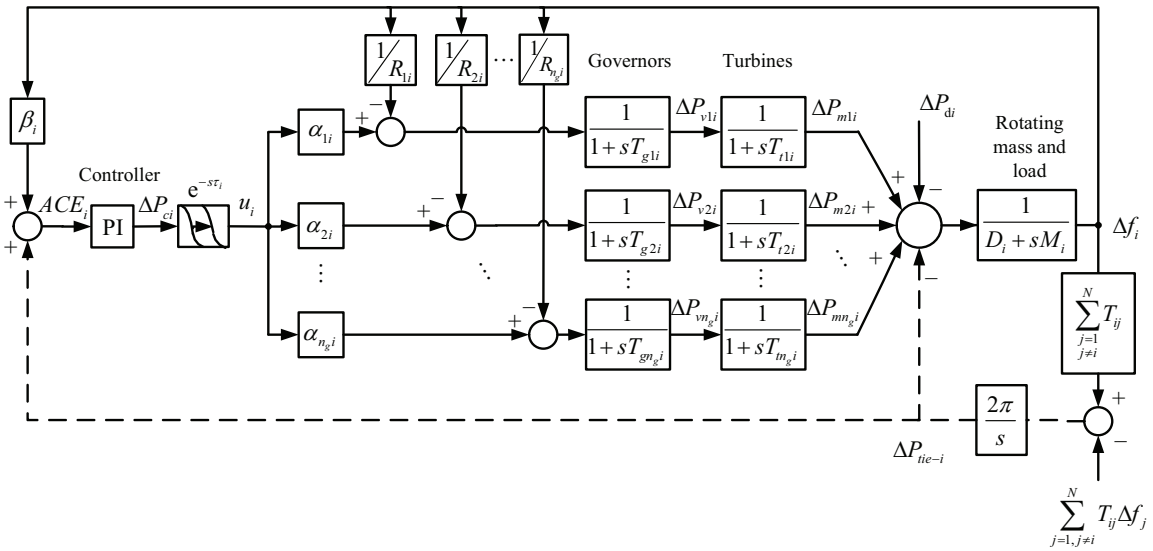

Fig. 1: Single-area (without dotted lines) and Multi-area (with dotted lines) LFC control structure.

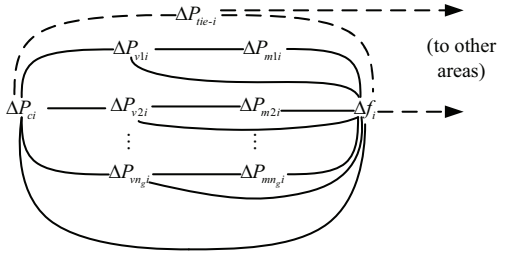

Fig. 2: Connections of state variables of single-area (without dotted lines) and multi-area (with dotted lines) LFC.

$$\boldsymbol{\Phi} = \begin{bmatrix} \boldsymbol{\Phi}_{11} & \boldsymbol{\Phi}_{12} & \boldsymbol{S} & \tau\boldsymbol{A}^\top\boldsymbol{R} \\ \boldsymbol{\Phi}_{12}^\top & \boldsymbol{\Phi}_{22} & -\boldsymbol{S}+\boldsymbol{R} & \tau\boldsymbol{A}_d^\top\boldsymbol{R} \\ \boldsymbol{S}^\top & -\boldsymbol{S}^\top+\boldsymbol{R} & -\boldsymbol{R}-\boldsymbol{Q}_2 & \boldsymbol{0} \\ \tau\boldsymbol{R}\boldsymbol{A} & \tau\boldsymbol{R}\boldsymbol{A}_d & \boldsymbol{0} & -\boldsymbol{R} \end{bmatrix} \prec 0 \quad (4)$$

where $\boldsymbol{\Phi}_{11} = \boldsymbol{P}\boldsymbol{A} + \boldsymbol{A}^\top\boldsymbol{P} + \boldsymbol{Q}_1 + \boldsymbol{Q}_2 - \boldsymbol{R}$, $\boldsymbol{\Phi}_{12} = \boldsymbol{P}\boldsymbol{A}_d + \boldsymbol{R} - \boldsymbol{S}$ and $\boldsymbol{\Phi}_{22} = -(1-\mu)\boldsymbol{Q}_1 - 2\boldsymbol{R} + \boldsymbol{S}^\top + \boldsymbol{S}$.

Since the state-of-art LMI solvers have very limited ability to solve large-scale LMIs, Theorem 1 poses a great computational challenge to the application of DDSA to real-world systems. In the following sections, we describe the structure-exploiting techniques based on Theorem 1, but the proposed techniques are not restricted to Theorem 1 and can also be applied to other LMI based delay-dependent stability criteria.

III. Chordal-structured Matrix Decomposition

This section provides theory foundation for subsequent discussions. Some concepts and properties related to the chordal graph are reviewed at first. Then the theorem of chordal-structured matrix decomposition is described. Finally, several useful lemmas are presented and proved. The proofs can be skipped for pure application purpose.

A. Theoretical Background

Let $\mathbb{M}_n$ denote the set of $n \times n$ matrices, and the symmetric subset of $\mathbb{M}_n$ is $\mathbb{S}_n$. Every $\boldsymbol{A} \in \mathbb{M}_n$ is naturally associated with an undirected graph $G(V, E)$ where the vertex set $V = \{1, 2, \cdots, n\}$ and the edge set $E = \{(i,j) \in V \times V : i \neq j, |[\boldsymbol{A}]_{ij}| + |[\boldsymbol{A}]_{ji}| \neq 0\}$ where $[\boldsymbol{A}]_{ij}$ denotes the $(i,j)^{\text{th}}$ element of $\boldsymbol{A}$. If $(i,j) \in E$, vertex i and j are said to be adjacent. The set of all vertices adjacent to vertex i is denoted by $adj_G(i)$. A graph is called complete if every pair of its vertices are adjacent. For any vertex subset $V' \subseteq V$, the subgraph induced by V' is a graph $G'(V', E')$ with $E' = E \cap (V' \times V')$. A clique is a subset of vertices of an undirected graph such that its induced subgraph is complete, and a clique is maximal if it is not a proper subset of another clique. Let $[n_1, n_2, \cdots, n_k]$ be a path of length k from vertex n_1 to vertex n_k, i.e. $(n_i, n_{i+1}) \in E$ for $1 \leq i \leq k-1$. Specially, a cycle is a path with $n_1 = n_k$. A graph is connected if there are paths containing each pair of vertices. A tree is an undirected connected graph with no cycles. In addition, a chord of a cycle is any edge joining two nonconsecutive vertices of the cycle.

The concept of chordal graph is central in this paper:

***Definition** 1 ([23]):* An undirected graph is chordal if every cycle of length greater than three has a chord.

Other than the definition given above, the chordal graph can be characterized in several different ways [23]. The characterization of clique trees is of concern in this paper. Let $G(V, E)$ be any graph. The set of all maximal cliques of G is denoted by $\mathcal{C} = \{C_1, C_2, \cdots, C_p\}$. Consider a tree $\mathcal{T}(\mathcal{C}, \mathcal{E})$ with vertices from $\mathcal{C}$ and edges from $\mathcal{E} \subseteq \mathcal{C} \times \mathcal{C}$. We call $\mathcal{T}(\mathcal{C}, \mathcal{E})$ a clique tree if it satisfies the clique-intersection property (**CIP**), i.e. for each pair of distinct maximal cliques C_i, $C_j \in \mathcal{C}$, the set $C_i \cap C_j$ is contained in every maximal clique on the path connecting C_i and C_j in the tree. In fact, the existence of a clique graph is equivalent to chordality:

***Lemma** 1 ([23]):* A connected undirected graph G is chordal if and only if there exists a clique tree $\mathcal{T}(\mathcal{C}, \mathcal{E})$.

On the other hand, given a graph $G(V,E)$, the set of matrices associated with this graph is denoted by $\mathbb{M}_n(E) = \{\boldsymbol{A} \in \mathbb{M}_n : [\boldsymbol{A}]_{ij} = 0 \text{ if } i \neq j \ \& \ (i,j) \notin E\}$. The symmetric subset of $\mathbb{M}_n(E)$ is denoted by $\mathbb{S}_n(E) = \mathbb{M}_n(E) \cap \mathbb{S}_n$. Further denote $\mathbb{S}_n^C = \{\boldsymbol{X} \in \mathbb{S}_n : [\boldsymbol{X}]_{ij} = 0 \text{ if } (i,j) \notin C \times C\}$ for every $C \subseteq V$. Let $\boldsymbol{E}_{ij}$ denote the appropriately dimensioned matrix with the $(i,j)^{\text{th}}$ element 1 and others 0.

Now we are ready to state the theorem of chordal-structured matrix decomposition as follows:

Theorem 2 ([24]): Given a chordal graph $G(V,F)$ with its maximal cliques $\mathcal{C} = \{C_1, C_2, \cdots, C_p\}$. $\mathcal{T}(\mathcal{C}, \mathcal{E})$ is a clique tree. Define $J(C) = \{(i,j) \in C \times C : i \leq j\}$ for every $C \subseteq V$ and

$$\Lambda = \{(g,h,k,l) : (g,h) \in J(C_k \cap C_l), (C_k, C_l) \in \mathcal{E}\}. \quad (5)$$

Any $\boldsymbol{A} \in \mathbb{S}_n(F)$ can be decomposed into $\tilde{\boldsymbol{A}}^k \in \mathbb{S}_n^{C_k} (k = 1,2,\cdots,p)$ such that $\boldsymbol{A} = \sum_{k=1}^p \tilde{\boldsymbol{A}}^k$. Then $\boldsymbol{A} \succcurlyeq \boldsymbol{0}$ if and only if the system of LMIs

$$\tilde{\boldsymbol{A}}^k - \tilde{\boldsymbol{L}}^k(\boldsymbol{z}) \succcurlyeq \boldsymbol{0} \ (k = 1,2,\cdots,p) \quad (6)$$

is feasible. Here $\boldsymbol{z} = (z_{ghkl} : (g,h,k,l) \in \Lambda)$ denotes a vetor variable consisting of $z_{ghkl} ((g,h,k,l) \in \Lambda)$, and

$$\tilde{\boldsymbol{L}}^k(\boldsymbol{z}) = - \sum_{(i,j,h):(i,j,h,k) \in \Lambda} \boldsymbol{E}_{ij} z_{ijhk} + \sum_{(i,j,l):(i,j,k,l) \in \Lambda} \boldsymbol{E}_{ij} z_{ijkl} \quad (7)$$

for every $\boldsymbol{z} = (z_{ghkl} : (g,h,k,l) \in \Lambda)$.
Note that the PSD condition on $\tilde{\boldsymbol{A}}^k - \tilde{\boldsymbol{L}}^k(\boldsymbol{z})$ is equivalent to the PSD condition on the submatrix indexed by C_k. Therefore, Theorem 2 transforms the PSD condition on a single $n \times n$ matrix into the PSD condition on multiple smaller matrices. When the sizes of the maximal cliques are much smaller than the size of $\boldsymbol{A}$, this transformation will bring significant computational advantages. For an arbitrary symmetric matrix $\boldsymbol{A}$, the corresponding graph $G(V,E)$ is not necessarily chordal. In this case, we can always find a chordal extension of $G(V,E)$, i.e. a chordal graph $G(V,F)$ with $F \supseteq E$, by adding some edges. Clearly, $\boldsymbol{A} \in \mathbb{S}_n(F)$. Then Theorem 2 can be readily applied to $G(V,F)$ and $\boldsymbol{A}$.

B. Useful Lemmas

Next, we present several lemmas which play vital roles in application of Theorem 2 to DDSA. The proofs are included in the Appendix B.

Lemma 2: Given an undirected chordal graph $G(V,F)$ with its maximum cliques $\mathcal{C} = \{C_1, C_2, \cdots, C_p\}$. For any symmetric matrix $\boldsymbol{A} \in \mathbb{S}_n(F)$ and matrix $\boldsymbol{B} \in \mathbb{M}_n(H)$ where

$$H = \{(i,j) \in V \times V : i \neq j, \\ \exists \ r, \ i,j \in C_r, \ adj_G(i) \setminus C_r = adj_G(j) \setminus C_r\}, \quad (8)$$

$\boldsymbol{AB} \in \mathbb{M}_n(F)$ and $\boldsymbol{BA} \in \mathbb{M}_n(F)$.

Remark 1: Lemma 2 characterizes the structure of $\boldsymbol{B}$ allowing $\boldsymbol{AB}$ and $\boldsymbol{BA}$ to inherit the chordal sparsity pattern of $\boldsymbol{A}$. In fact, two categories of elements (i,j) satisfy the defining property stated in (8). First, i and j are inner vertices of the same maximal clique C_r, i.e. $adj_G(i) \subseteq C_r$ and $adj_G(j) \subseteq C_r$. Second, vertex i and j are adjacent to the same vertices outside the clique they both belong to. If nonzero elements of $\boldsymbol{B}$ are only allowed at (i,j) from above two categories, the multiplication $\boldsymbol{AB}$ will not create new nonzero elements outside F thus inherit the sparsity of $\boldsymbol{A}$.

Lemma 3: Given m chordal graphs $G^{(k)}(V^{(k)}, F^{(k)})$, $k = 1,2,\cdots,m$ of exactly the same structure, the maximum cliques of the k^{th} graph are denoted by $\mathcal{C}^{(k)} = \{C_1^{(k)}, C_2^{(k)}, \cdots, C_p^{(k)}\}$. Another graph $G(V,F)$ is constructed as follows:

$$V = \cup_{k=1}^m V^{(k)} \quad (9)$$

$$F = \{(i,j) \in \cup_{r=1}^p (C_r \times C_r) : i \neq j\} \quad (10)$$

where $C_r = \cup_{k=1}^m C_r^{(k)}$. Then $G(V,F)$ is a chordal graph with $\mathcal{C} = \{C_1, C_2, \cdots, C_p\}$ being the maximum cliques.

Remark 2: Lemma 3 states that a large chordal graph can be constructed from a group of small chordal graphs with the same structure by merging corresponding maximum cliques of small chordal graphs.

Lemma 3 is useful when dealing with the block matrix with each block having the same chordal sparsity pattern. The following corollary is a direct consequence of Lemma 3.

Corollary 1: Let

$$\boldsymbol{\Phi} = \begin{bmatrix} \boldsymbol{\Phi}_{11} & \cdots & \boldsymbol{\Phi}_{1m} \\ \vdots & \ddots & \vdots \\ \boldsymbol{\Phi}_{m1} & \cdots & \boldsymbol{\Phi}_{mm} \end{bmatrix} \quad (11)$$

be a $nm \times nm$ symmetric matrix with each block $\boldsymbol{\Phi}_{ij} \in \mathbb{M}_n$. $G(V,F)$ is a chordal graph with vertices $V = \{1,\cdots,n\}$ and maximum cliques $\mathcal{C} = \{C_1, C_2, \cdots, C_p\}$. If $\boldsymbol{\Phi}_{ij} \in \mathbb{M}_n(F), \forall 1 \leq i,j \leq m$, then $\boldsymbol{\Phi}$ is associated with chordal graph $G'(V',F')$, i.e. $\boldsymbol{\Phi} \in \mathbb{S}_{nm}(F')$ where $V' = \cup_{k=0}^{m-1}(kn + V)$ and $F' = \{(i,j) \in \cup_{r=1}^p (\cup_{k=0}^{m-1}(kn + C_r)) \times (\cup_{k=0}^{m-1}(kn + C_r)) : i \neq j\}$. $G'(V',F')$ is a chordal graph with

$$C_r' = \cup_{k=0}^{m-1}(kn + C_r), r = 1,\cdots,p \quad (12)$$

being the maximal cliques.

Based on Corollary 1, we then discuss a more complex situation with the $\boldsymbol{\Phi}_{11}$ block in (11) being fully dense and other blocks following the same chordal sparsity pattern.

Lemma 4: Let $\boldsymbol{\Phi}$ be the $nm \times nm$ block symmetric matrix shown in (11) where $\boldsymbol{\Phi}_{11}$ is fully dense. $\boldsymbol{\Phi}_{ij}, \ i + j > 2$, is associated with graph $G(V,F)$, i.e. $\boldsymbol{\Phi}_{ij} \in \mathbb{M}_n(F), \forall i + j > 2$. $G(V,F)$ is a chordal graph with vertices $V = \{1,\cdots,n\}$ and maximal cliques $\mathcal{C} = \{C_1, C_2, \cdots, C_p\}$. Define $\hat{V} = \cup_{1 \leq r,t \leq p}(C_r \cap C_t)$. Then $\boldsymbol{\Phi}$ is associated with chordal graph $G^*(V^*,F^*)$, i.e. $\boldsymbol{\Phi} \in \mathbb{S}_{nm}(F^*)$ where $V^* = \cup_{k=0}^{m-1}(kn + V)$ and $F^* = \{(i,j) \in \cup_{r=0}^p C_r^* \times C_r^* : i \neq j\}$ with

$$C_0^* = V \cup \left(\cup_{k=1}^{m-1}(kn + \hat{V})\right) \quad (13)$$

$$C_r^* = \cup_{k=0}^{m-1}(kn + C_r), \ r = 1,\cdots,p. \quad (14)$$

Accordingly, $\mathcal{C}^* = \{C_0^*, C_1^*, \cdots, C_p^*\}$ are the maximal cliques of $G^*(V^*,F^*)$.

Remark 3: The structure of $\boldsymbol{\Phi}$ described in Lemma 4 is what will be encountered in the DDSA. If the sizes of $\hat{V}$ and $C_r, r = 1,\cdots,p$ are much smaller than n, the sizes of $C_r^*, r =$

$0, \cdots, p$ would be much smaller than nm. Then Theorem 2 can be employed to decompose the PSD condition on $\mathbf{\Phi}$ into PSD conditions on much smaller matrices.

IV. Structure-exploiting Delay-dependent Stability Analysis of Load Frequency Control

This section presents the techniques to exploit chordal sparsity and symmetry in DDSA of LFC.

A. Exploiting Chordal Sparsity

In practical problems, like power system LFC, the system matrices $\boldsymbol{A}$ and $\boldsymbol{A}_d$ exhibit strong sparsity. We introduce the aggregate system matrix

$$\bar{\boldsymbol{A}} = |\boldsymbol{A}| + \mathbf{1}_n |\boldsymbol{A}_d| \tag{15}$$

where $\mathbf{1}_n$ denotes the $n \times n$ all-ones matrix, and the aggregate sparsity pattern graph $G(V, E)$ with $V = \{1, 2, \cdots, n\}$ and $E = \{(i, j) \in V \times V : i \neq j, |[\bar{\boldsymbol{A}}]_{ij}| + |[\bar{\boldsymbol{A}}]_{ji}| \neq 0\}$. The sparsity of the system matrices is thus represented by the sparsity of graph $G(V, E)$. However, the sparsity of the system matrices do not readily lead to the sparsity of the LMI (3) and (4) due to the full flexibility of weighting matrices. To take advantages of the sparsity of system matrices, we need to properly restrict the structure of weighting matrices $\boldsymbol{Q}_1$, $\boldsymbol{Q}_2$, $\boldsymbol{R}$ and $\boldsymbol{S}$ so that the LMI (3) and (4) can inherit the sparsity from system matrices. This idea is made precise by the following theorem.

***Theorem** 3:* Let $G(V, F)$ be a chordal extension of the aggregate sparsity pattern graph $G(V, E)$ of system (1) as defined above. $\mathcal{C} = \{C_1, C_2, \cdots, C_p\}$ are the maximal cliques of $G(V, F)$. H is the edge set defined in (8). Let $\boldsymbol{P} \in \mathbb{S}_n$, $\boldsymbol{Q}_1, \boldsymbol{Q}_2 \in \mathbb{S}_n(F)$, $\boldsymbol{R} \in \mathbb{S}_n(H)$ and $\boldsymbol{S} \in \mathbb{M}_n(F)$. Then $\mathbf{\Psi}$ (3) is associated with the chordal graph $G'(V', F')$ defined in Corollary 1 with $m = 2$, and $\mathbf{\Phi}$ (4) is associated with the chordal graph $G^*(V^*, F^*)$ defined in Lemma 4 with $m = 4$.

Proof: According to Lemma 2, $\boldsymbol{Q}_1, \boldsymbol{Q}_2 \in \mathbb{S}_n(F)$, $\boldsymbol{R} \in \mathbb{S}_n(H)$ and $\boldsymbol{S} \in \mathbb{M}_n(F)$ imply that all blocks of $\mathbf{\Phi}$ except $\mathbf{\Phi}_{11}$ are in $\mathbb{M}_n(F)$, and $\mathbf{\Phi}_{11}$ is fully dense in general, i.e. $\mathbf{\Phi}$ satisfies the conditions in Lemma 4. Therefore, $\mathbf{\Phi} \in \mathbb{S}_{4n}(F^*)$ where the chordal graph $G^*(V^*, F^*)$ is defined in Lemma 4 with $m = 4$. Moreover, since each block of $\mathbf{\Psi}$ belongs to $\mathbb{M}_n(F)$, $\mathbf{\Psi} \in \mathbb{S}_{2n}(F')$ with the chordal graph $G'(V', F')$ defined with $m = 2$ in Corollary 1. ■

***Remark** 4:* As the consequence of Theorem 3, all matrices except $\boldsymbol{P}$ in Theorem 1 with PSD conditions are associated with related chordal graphs, i.e. $\boldsymbol{Q}_1, \boldsymbol{Q}_2, \boldsymbol{R} \in \mathbb{S}_n(F)$, $\mathbf{\Psi} \in \mathbb{S}_{2n}(F')$ and $\mathbf{\Phi} \in \mathbb{S}_{4n}(F^*)$. Therefore, Theorem 2 can be employed to decompose these PSD conditions into smaller ones.

The effects of enforcing chordal sparsity on weighting matrices as described in Theorem 3 are twofold. First, the number of decision variables is reduced; Second, the sizes of the PSD conditions are reduced. Both effects contribute to the improvement of numerical tractability. However, by restricting the structure of weighting matrices $\boldsymbol{Q}_1, \boldsymbol{Q}_2, \boldsymbol{R}$ and $\boldsymbol{S}$, the obtained stability criterion becomes more conservative than Theorem 1, which is the price has to be paid for improving the numerical tractability. The conservatism brought by the structure restriction of weighting matrices will be assessed by numerical studies in section V. Note that we do not enforce chordal sparsity on $\boldsymbol{P}$ due to the experience that enforcing chordal sparsity on $\boldsymbol{P}$ will make the stability criterion overly conservative thus useless in practice. This is in stack contrast to the pure control theory paper [20] which enforces sparsity on $\boldsymbol{P}$ and exploits the sparsity of $\boldsymbol{A}^T\boldsymbol{P} + \boldsymbol{P}\boldsymbol{A}$.

Consider the single-area LFC with turbine governor model shown in Fig. 1 as an example. It can be verified by definition that the graph related to $\bar{\boldsymbol{A}}$ of single-area LFC shown in Fig. 3 is already a chordal graph without adding edges, i.e. $F = E$. The maximal cliques of this chordal graph are $\mathcal{C}_i = \{\Delta P_c, \Delta f, \Delta P_{vi}, \Delta P_{mi}\}, i = 1, 2, \cdots, n$. The edges that belong to set H defined in (8) are shown with red dotted lines. By restricting the structures of weighting matrices as stated in Theorem 3, the $(2n_g+2) \times (2n_g+2)$ PSD conditions on $\boldsymbol{Q}_1, \boldsymbol{Q}_2, \boldsymbol{R}$ can all be reduced to 4×4 PSD conditions on their submatrices indexed by the maximal cliques. The PSD conditions on Ψ and Φ can also be reduced according to the maximal cliques of $G'(V', F')$ and $G^*(V^*, F^*)$ given in Corollary 1 and Lemma 4, respectively.

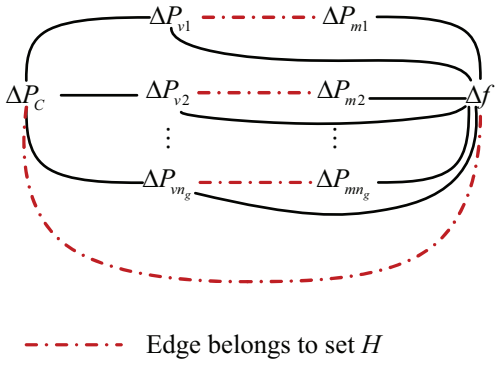

Fig. 3: Chordal graph for single-area LFC. The maximal cliques are $\mathcal{C}_i = \{\Delta P_c, \Delta f, \Delta P_{vi}, \Delta P_{mi}\}, i = 1, 2, \cdots, n$.

B. Exploiting Symmetry

Due to the full flexibility of weighting matrix $\boldsymbol{P}$, the DDSA is still computationally intensive even when chordal sparsity is exploited. We need to further restrict the structure of $\boldsymbol{P}$ by exploiting symmetry.

The basic idea rests on the observation that many elements of matrix $\boldsymbol{P}$ take very similar values when we directly conduct DDSA using Theorem 1 on a small-scale LFC system. The fundamental reason for this phenomenon is the highly symmetric structure of LFC control loops shown in Fig. 2 and similar parameters of generation units. Note that $\boldsymbol{P}$ is the weighting matrix related to the first term in LKF (2). If the "nature" of the state variable pair (i, j) is the same as that of state variable pair (k, l), $[\boldsymbol{P}]_{ij}$ and $[\boldsymbol{P}]_{kl}$ should take the similar values. For example, in a single-area LFC, assume that unit i and unit j have similar parameters. In the LKF of the system, the coefficients of $\Delta f \Delta P_{vi}$ and $\Delta f \Delta P_{vj}$ should take similar values because ΔP_{vi} and ΔP_{vj} are of the same relation to

TABLE I: Orbits of Group Σ Operating on Index Pair (i,j)

(i,j)	$\mathcal{O}(i,j)$
$i,j \notin \mathcal{I}_g$	$\{(i,j)\}$
$(i, i^l_{g_k}),\ i \notin \mathcal{I}_g$	$\{(i, i^l_{g_h}) : g_h \sim g_k\}$
$(i^l_{g_k}, i),\ i \notin \mathcal{I}_g$	$\{(i^l_{g_h}, i) : g_h \sim g_k\}$
$(i^l_{g_k}, i^m_{g_k})$	$\{(i^l_{g_h}, i^m_{g_h}) : g_h \sim g_k\}$
$(i^l_{g_k}, i^m_{g_h}), g_k \neq g_h$	$\{(i^l_{g_{k'}}, i^m_{g_{h'}}) : g_{k'} \sim g_k, \sim g_{h'} \sim g_h, k' \neq h'\}$

Δf. It is also the case for $\Delta f \Delta P_{mi}$ and $\Delta f \Delta P_{mj}$, $\Delta P_c \Delta P_{vi}$ and $\Delta P_c \Delta P_{vj}$, $\Delta P_c \Delta P_{mi}$ and $\Delta P_c \Delta P_{mj}$, etc. Moreover, we conjecture that although the parameters of generation units are different in practice, enforcing the above-mentioned symmetry on $\boldsymbol{P}$ would not introduce much conservatism to the results of DDSA.

To formalize the idea described above, we need to introduce the notion of permutation group. A permutation σ is a bijective map from set $\{1, 2, \cdots, n\}$ to itself. For our propose, here n is the dimension of the system matrix. A set of permutations Σ is called a permutation group if it is closed under composition and contains the identity map. The permutation group of concern to us is constructed as follows:

1) Endow the set of all generation units $\{g_1, \cdots, g_{n_g}\}$ with an equivalence relation $\sim$. We say $g_h \sim g_k$ if and only if they belong to the same control area and their turbine-governor systems have similar structure and parameters.
2) Let $\{i^1_{g_k}, \cdots, i^p_{g_k}\}$ be the indices of the state variables related to the turbine-governor system of generation unit g_k, and $\mathcal{I}_g = \bigcup_{\forall k,l} \{i^l_{g_k}\}$. Define the permutation group Σ as the set of all permutations satisfying $\sigma(i) = i$ if $i \notin \mathcal{I}_g$ and $\forall g_k$, $\exists g_h \sim g_k$ such that $\sigma(i^l_{g_k}) = i^l_{g_h}, \forall 1 \leq l \leq p$.

The definition of the permutation group given above allows us to establish a equivalence relation on pairs of state variables: $(i,j) \sim (k,l)$ if and only if there exists $\sigma \in \Sigma$ such that $k = \sigma(i)$ and $l = \sigma(j)$. Hence the vague idea of "state variable pair (i,j) and (k,l) are of the same nature" is precisely characterized by the equivalence relation $(i,j) \sim (k,l)$. As a result, $[\boldsymbol{P}]_{ij}$ and $[\boldsymbol{P}]_{\sigma(i)\sigma(j)}$ are expected to take the same value, i.e. $[\boldsymbol{P}]_{ij} = [\boldsymbol{P}]_{\sigma(i)\sigma(j)}, \forall \sigma \in \Sigma$ and we say $\boldsymbol{P}$ is Σ-invariant. To precisely characterize the structure of $\boldsymbol{P}$, we need to introduce the concept of the orbit. The orbit to which the pair (i,j) belong under the permutation group Σ is given by

$$\mathcal{O}(i,j) = \{(\sigma(i), \sigma(j)) | \sigma \in \Sigma\}. \tag{16}$$

It is well known that the orbits partition the set on which the group operates [25], i.e. the set $\{1, \cdots, n\} \times \{1, \cdots, n\}$ is partitioned into several orbits $\mathcal{O}_1, \mathcal{O}_2, \cdots, \mathcal{O}_r$. Based on the definition of the permutation group Σ, we explicitly show the structures of the orbits in Table I. Matrix $\boldsymbol{P}$ thus takes the same value on each orbit. For every $k \in \{1, \cdots, r\}$ we define $\hat{\boldsymbol{B}}_k \in \{0,1\}^{n \times n}$ by $[\hat{\boldsymbol{B}}_k]_{ij} = 1$ if $(i,j) \in \mathcal{O}_k$ and $[\hat{\boldsymbol{B}}_k]_{ij} = 0$ otherwise. Then $\hat{\boldsymbol{B}}_1, \cdots, \hat{\boldsymbol{B}}_r$ form a basis of the space of Σ-invariant matrices (not necessarily symmetric). The basis of the space of symmetric Σ-invariant matrices can then be obtained by setting $\boldsymbol{B}_k = \hat{\boldsymbol{B}}_h + \hat{\boldsymbol{B}}_l$ if $\hat{\boldsymbol{B}}^T_h = \hat{\boldsymbol{B}}_l$ and $\boldsymbol{B}_k = \hat{\boldsymbol{B}}_k$ if $\hat{\boldsymbol{B}}^T_k = \hat{\boldsymbol{B}}_k$. Therefore, $\boldsymbol{P}$ is parametrized by $\boldsymbol{P} = \sum_{k=1}^{p} p_k \boldsymbol{B}_k$.

To exemplify the effects of the above procedure, we first consider a single-area LFC with three generation units. The turbine governor models of all generating units are as shown in Fig. 1 and we assume all generating units are all similar to each other. Then parametrized matrix $\boldsymbol{P} = \sum_{k=1}^{13} p_k \boldsymbol{B}_k$ is depicted in Fig. 4. The number of decision variables are reduced from $(2n_g+2)(2n_g+3)/2$ to 13.

	ΔP_c	Δf	ΔP_{v1}	ΔP_{v2}	ΔP_{v3}	ΔP_{m1}	ΔP_{m2}	ΔP_{m3}
ΔP_c	p_1	p_2	p_3	p_3	p_3	p_4	p_4	p_4
Δf	p_2	p_5	p_6	p_6	p_6	p_7	p_7	p_7
ΔP_{v1}	p_3	p_6	p_8	p_9	p_9	p_{10}	p_{11}	p_{11}
ΔP_{v2}	p_3	p_6	p_9	p_8	p_9	p_{11}	p_{10}	p_{11}
ΔP_{v3}	p_3	p_6	p_9	p_9	p_8	p_{11}	p_{11}	p_{10}
ΔP_{m1}	p_4	p_7	p_{10}	p_{11}	p_{11}	p_{12}	p_{13}	p_{13}
ΔP_{m2}	p_4	p_7	p_{11}	p_{10}	p_{11}	p_{13}	p_{12}	p_{13}
ΔP_{m3}	p_4	p_7	p_{11}	p_{11}	p_{10}	p_{13}	p_{13}	p_{12}

Fig. 4: Structure of the symmetric Σ-invariant matrix $\boldsymbol{P}$ for a single-area LFC with three generation units

The same procedure can be readily applied to three-area LFC. We consider a three-area LFC scheme with three generation units in each area and generation units in each area are assumed to be similar to each other. To simplify the presentation, we partition the weighting matrix $\boldsymbol{P}$ into six independent blocks, i.e.

$$\boldsymbol{P} = \begin{bmatrix} \boldsymbol{P}_{11} & \boldsymbol{P}_{12} & \boldsymbol{P}_{13} \\ \boldsymbol{P}^T_{12} & \boldsymbol{P}_{22} & \boldsymbol{P}_{23} \\ \boldsymbol{P}^T_{13} & \boldsymbol{P}^T_{23} & \boldsymbol{P}_{33} \end{bmatrix} \tag{17}$$

where $\boldsymbol{P}_{ii} (i = 1,2,3)$ represents the coefficients of quadratic term within the control area i, and $\boldsymbol{P}_{ij}$ denotes the coefficients of the cross-product term between area i and area j. Since the structure of $\boldsymbol{P}_{ii}$ is similar to that of single-area LFC, we only show the structure of $\boldsymbol{P}_{ij}$ in Fig. 5. The number of decision variables in $\boldsymbol{P}_{ij}$ is reduced from $(2n_g+3)^2$ to 25.

	ΔP_{cj}	Δf_j	$\Delta P_{\text{tie-}j}$	ΔP_{v1j}	ΔP_{v2j}	ΔP_{v3j}	ΔP_{m1j}	ΔP_{m2j}	ΔP_{m3j}
ΔP_{ci}	p_1	p_2	p_3	p_4	p_4	p_4	p_5	p_5	p_5
Δf_i	p_6	p_7	p_8	p_9	p_9	p_9	p_{10}	p_{10}	p_{10}
$\Delta P_{\text{tie-}i}$	p_{11}	p_{12}	p_{13}	p_{14}	p_{14}	p_{14}	p_{15}	p_{15}	p_{15}
ΔP_{v1i}	p_{16}	p_{17}	p_{18}	p_{19}	p_{19}	p_{19}	p_{20}	p_{20}	p_{20}
ΔP_{v2i}	p_{16}	p_{17}	p_{18}	p_{19}	p_{19}	p_{19}	p_{20}	p_{20}	p_{20}
ΔP_{v3i}	p_{16}	p_{17}	p_{18}	p_{19}	p_{19}	p_{19}	p_{20}	p_{20}	p_{20}
ΔP_{m1i}	p_{21}	p_{22}	p_{23}	p_{24}	p_{24}	p_{24}	p_{25}	p_{25}	p_{25}
ΔP_{m2i}	p_{21}	p_{22}	p_{23}	p_{24}	p_{24}	p_{24}	p_{25}	p_{25}	p_{25}
ΔP_{m3i}	p_{21}	p_{22}	p_{23}	p_{24}	p_{24}	p_{24}	p_{25}	p_{25}	p_{25}

Fig. 5: Structure of the symmetric Σ-invariant partial matrix $\boldsymbol{P}_{ij}$ for a three-area LFC with three generation units in each area

The symmetry-exploiting technique described above significantly reduces the number of decision variables, which contributes to the improvement of numerical tractability. However,

the structure restriction of weighting matrix $\boldsymbol{P}$ will also bring additional conservatism which will be assessed by numerical studies in section V.

C. Implementation Issues

The main steps of **structure-exploiting DDSA** are summarized as follows:

Step1. Obtain a chordal extension $G(V, F)$ and its maximal cliques of the aggregate sparsity pattern graph. This can be accomplished by performing a Cholesky factorization to $\bar{\boldsymbol{A}} + \bar{\boldsymbol{A}}^T + \epsilon \boldsymbol{I}$ (Here ϵ is any positive number to guarantee the positive definiteness of the matrix to be factorized) with approximate minimum degree ordering, i.e. $\bar{\boldsymbol{A}} + \bar{\boldsymbol{A}}^T + \epsilon \boldsymbol{I} = \boldsymbol{L}^T \boldsymbol{L}$. The sparsity pattern of the Cholesky factor defines the chordal extension and the maximal cliques, i.e. $F = \{(i, j) \in V \times V : i \neq j, |[\boldsymbol{L}]_{ij}| + |[\boldsymbol{L}]_{ji}| \neq 0\}$.

Step2. Obtain the edge set H defined in (8) and restrict the structure of $\boldsymbol{Q}_1, \boldsymbol{Q}_2, \boldsymbol{R}$ and $\boldsymbol{S}$ as: $\boldsymbol{R}, \boldsymbol{Q}_1, \boldsymbol{Q}_2 \in \mathbb{S}_n(H)$ and $\boldsymbol{S} \in \mathbb{M}_n(H)$. Note that although Theorem 3 only requires $\boldsymbol{Q}_1, \boldsymbol{Q}_2 \in \mathbb{S}_n(F)$ and $\boldsymbol{S} \in \mathbb{M}_n(F)$, we found that further restricting $\boldsymbol{Q}_1, \boldsymbol{Q}_2 \in \mathbb{S}_n(H)$ and $\boldsymbol{S} \in \mathbb{M}_n(H)$ does not bring much conservatism in practice. Under above structure restriction of the weighting matrices, Theorem 3 guarantees the existence of chordal sparsity in the LMIs of Theorem 1.

Step3. Identify the equivalence relation among generation units and the permutation group Σ on the indices of state variables, and find out the orbits $\mathcal{O}_1, \mathcal{O}_2, \cdots, \mathcal{O}_r$ according to Table I.

Step4. Find out the basis $\boldsymbol{B}_1, \cdots, \boldsymbol{B}_r$ of all possible weighting matrix $\boldsymbol{P}$ with desirable symmetry structure according to the orbits of permutation group Σ. Then $\boldsymbol{P}$ is restricted as $\boldsymbol{P} = \sum_{k=1}^{p} p_k \boldsymbol{B}_k$.

Step5. Form the LMIs in Theorem 1 and reformulate it with the chordal-structured matrix decomposition (Theorem 2). This step can be implemented conveniently using existing software package SparseCoLO which automatically detects the chordal structure in general semidefinite programming (SDP) and reformulates the SDP to facilitate the solution using standard solvers [24].

Step6. Solve the obtained new LMIs with standard LMI solvers.

It it worth mentioning that the above procedure is totally algorithmic and does not reply on specific models of turbine-governor systems and AGC controllers. Hence the proposed method is adaptive to different models employed. Fig. 6 shows the difference between the proposed structure-exploiting DDSA and the direct DDSA. In the structure-exploiting DDSA, the stability criterion is pre-processed by the sparsity and symmetry exploiting techniques before solved by the standard LMI solver. Whereas the stability criterion is directly sent to the solver without any processing in the direct DDSA. The practical effects of the pre-processing will be comprehensively assessed by numerical studies in the next section.

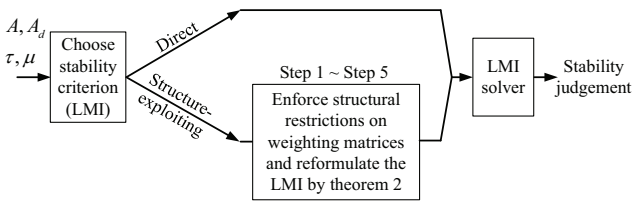

Fig. 6: Procedures of direct and structure-exploiting DDSA

V. Numerical Results

This section presents the numerical studies of the proposed structure-exploiting DDSA with comparison to the direct DDSA. The computational performance and introduced conservatism of the proposed structure-exploiting techniques are analyzed in details. The methods are implemented in MATLAB 2015b with YALMIP [26] as the modeling tool and SDPT3 [27] as the solver. SparseCoLO [24] is used to automates the chordal-structured matrix decomposition. The program runs on a Win8 PC with a 3.0 GHz CPU and 24 GB RAM.

The numerical tests are based on 10 unit 39 bus New England system (NE39). Larger test systems are constructed by directly scale up the NE39. For example, the 200 unit system is obtained by merging 20 NE39 systems. The generator inertia data can be found in [28] and the generator rated power and load demand are extracted from MATPOWER [29]. The load damping D in each synchronous area is assumed to be 1% total load/Hz. The typical values for droop characteristic R of each governor vary from 3% to 7% p.u./rated power. The turbine-governor system of each unit is modelled as in Fig. 1. The typical parameters for turbine-governor systems are $T_g = 0.08s$ and $T_t = 0.40s$ [15]. In every numerical test, the actual values for T_g, T_t and R are randomly generated in the range of $1 \pm \chi\%$ of the typical values given above. The value of χ varies from 0 to 50 in the tests to reflect the different degree of non-symmetry from parameter variation. The participation factors are also randomly selected between 0 and 1. Three-area test cases are obtained by connecting three single-area systems. The connection parameters are $T_{12} = 0.20$, $T_{13} = 0.25$, $T_{21} = 0.20$, $T_{23} = 0.12$, $T_{32} = 0.25$ and $T_{32} = 0.12$.

A. Computational Efficiency

The proposed structure-exploiting DDSA has been employed in both single-area and three-area LFC schemes. For single-area problems, the structure-exploiting techniques are applied to Theorem 1. For three-area problems, Theorem 1 is no longer applicable since three independent time delays exist in the whole system and Theorem 1 can only tackle single time delay. In this case, we apply the structure-exploiting technique to the stability criterion dealing with multiple constant delays proposed in our previous paper [4]. Fig. 7 shows the sparsity pattern of matrices in $\mathbb{S}_n(F)$ and $\mathbb{S}_n(H)$ decribed in Theorem 3 for single-area LFC with 50 generation units, and Fig. 8 depicts the sparsity pattern of matrices in $\mathbb{S}_n(F)$ and $\mathbb{S}_n(H)$ for three-area LFC with 20 generation units in each area. Both figures give us intuitive ideas about the sparsity of LFC loops

and the significant reduction in decision variables in weighting matrices when sparsity is exploited.

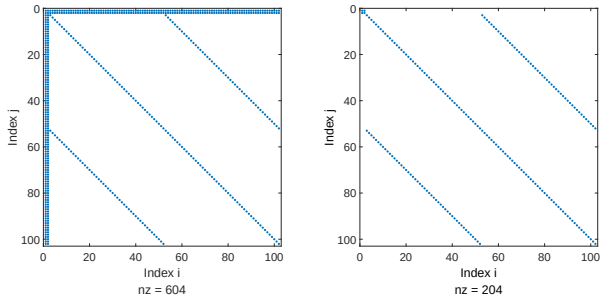

Fig. 7: Sparsity pattern of matrices in $\mathbb{S}_n(F)$ (left) and $\mathbb{S}_n(H)$ (right) described in Theorem 3 for single-area LFC with 50 generation units

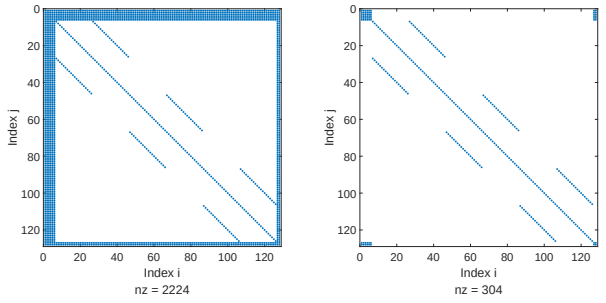

Fig. 8: Sparsity pattern of matrices in $\mathbb{S}_n(F)$ (left) and $\mathbb{S}_n(H)$ (right) described in Theorem 3 for three-area LFC with 20 generation units in each area

In the first group of tests, we fix the typical value of R to be 5% and set $\chi = 25$. Structure-exploiting DDSA and direct DDSA are conducted on LFC systems with different numbers of generation units. The computational performance statistics are summarized in Table II. Column 2 and 3 denote the numbers of generation units and the orders of the systems, respectively. Four statistics are used to assess the scale of the LMIs to be solved with both methods. **no. psd** and **max psd** denote the number and maximal size of PSD constraints, respectively. Since LMIs are transformed into standard SDP forms before solving by conic program solvers, the numbers of equality constraints (**m**) and decision variables (**n**) in standard primal form [27] are also taken as indicators of the problem scales. Moreover, **solver time** in Table II denotes the CPU time in seconds for SDPT3 to solve corresponding problems. As shown in Table II, by exploiting the chordal sparsity in DDSA, the numbers of PSD constraints increase whereas the sizes of PSD constraints decrease. Note that Theorem 3 only proves the existence rather than the uniqueness of the chordal structure in the LMIs after restricting the structure of the weighting matrices. SparseCoLO automatically selects a "good" chordal extension by merging some maximal cliques in the cliques tree to balance the increase in the number and decrease in the size of PSD constraints [30]. In general, by exploiting both chordal sparsity and symmetry, the decrease of m and n showed in Table II indicates the significant reduction in the scales of LMIs, which is further reflected in the solver time of each problem. For both single-area and multi-area LFC, direct DDSA is numerically tractable for systems with less than around 40 generation units, whereas structure-exploiting DDSA applies to systems with hundreds of generation units. For problems solvable by both methods, the solver time of structure-exploiting DDSA is two orders of magnitude less than that of direct DDSA. In a real-world power system, there could be hundreds of generation units. The improvement of the numerical tractability of the DDSA method would allow more detailed modeling for each control area, which increases the accuracy and reliability of the results of DDSA.

B. Evaluation of Additional Conservatism

To exploit chordal sparsity and symmetry in DDSA, structure restrictions are enforced on the weighting matrices, which inevitably brings additional conservatism. If too much conservatism is introduced, the method could become useless in practice. In the second group of tests, we evaluate the introduced conservatism by comparing the delay margins (stable delay region) obtained by the structure-exploiting DDSA and the direct DDSA on relatively small-scale systems. The typical value of R and χ are also set to be 5% and 25, respectively. Table. III reports the comparison of delay margins by two methods on single-area LFC with ten generation units under different parameters of the PI controller. The results show that the delay margins obtained by the structure-exploiting DDSA ($\boldsymbol{\tau_{se}}$) are uniformly larger than 90% of the delay margins by the direct DDSA ($\boldsymbol{\tau_{dr}}$), which indicates that the structure-exploiting techniques only introduce minor conservatism. Table IV lists the side lengths of the cubic stable delay region of three-area LFC obtained by both methods. For presentation simplicity, each control area is assumed to have the same PI parameters. The results in Table IV also confirm the conclusion that the structure-exploiting techniques only introduce minor conservatism. These tests numerically validate the conjecture we raised in section-IV-B. To better understand the underlying mechanism, we compare the mesh plots of obtained weighting matrices $\boldsymbol{P}$ and $\boldsymbol{Q}_1$ by two methods in Fig. 9 and Fig. 10. Both figures show that the overall structure of weighting matrices obtained by the structure-exploiting DDSA looks very similar to that of weighting matrices obtained by the direct DDSA. In other words, the proposed structure restrictions on weighting matrices are not very restrictive, so the structure-exploiting techniques only bring minor conservatism. Fig. 11 shows the comparison of frequency deviation for 0.1 p.u. step load disturbance of single-area LFC with τ_{se} and τ_{dr} in Table III. As shown in the time-domain simulation, both τ_{se} and τ_{dr} are conservative approximation to the underlying true delay margins, but τ_{se} possesses a little more conservatism than τ_{dr}.

In the following, we further define the degree of additional conservatism as

$$\rho_c = 1 - \frac{\tau_{se}}{\tau_{dr}}. \tag{18}$$

In the third group of tests, we investigate the sensitivity of ρ_c to the parameter $\chi\%$ and the typical value of R. The tests are performed on 10-unit single-area LFC. The

TABLE II: Comparison of Computational Performance of the Direct and Structure-exploiting DDSA

	ng	ord.	Direct DDSA					Stucture-exploiting DDSA				
			no. psd	max psd	m	n	solver time (s)	no. psd	max psd	m	n	solver time (s)
1-area	30	62	6	248	11656	92256	387.77	157	66	876	12734	2.03
	50	102	6	408	31416	249696	inf. (out of mem.)	257	106	1436	29154	4.51
	150	202	6	808	122816	979296	inf. (out of mem.)	507	206	2836	98204	19.03
	200	402	6	1608	485616	3878496	inf. (out of mem.)	1007	406	5636	356304	89.11
	500	1002	6	4008	3014016	24096096	inf. (out of mem.)	2507	1002	14036	2090604	827.32
3-area	3*10	68	8	476	16422	258944	810.77	280	100	1738	22917	5.88
	3*20	128	8	896	57792	917504	inf. (out of mem.)	551	146	3225	54449	30.30
	3*40	248	8	1736	216132	3444224	inf. (out of mem.)	1091	266	5954	164262	136.61
	3*60	368	8	2576	475272	7583744	inf. (out of mem.)	1631	386	8640	331484	404.87

TABLE III: Comparison of Delay Margins (seconds) by Two Methods on Single-area LFC with 10 Generation Units

(K_P, K_I)	τ_{se}	τ_{dr}	ratio
(0.05,0.05)	27.1765	28.5269	95.27%
(0.05,0.1)	13.4079	13.8895	96.53%
(0.05,0.15)	8.8376	8.9960	98.24%
(0.1,0.05)	26.3379	27.8265	94.65%
(0.1,0.1)	12.9913	14.1550	91.78%
(0.1,0.15)	8.5794	9.2047	93.21%

TABLE IV: Comparison of length of the Cubic Stable Delay Region (seconds) by Two Methods on Three-area LFC with 10 Generation Units in Each Area

(K_P, K_I)	τ_{se}	τ_{dr}	ratio
(0.05,0.05)	25.4993	26.4615	96.36%
(0.05,0.1)	12.5912	12.7927	98.43%
(0.05,0.15)	8.2242	8.2516	99.67%
(0.1,0.05)	24.6634	25.7419	95.81%
(0.1,0.1)	12.1820	13.0518	93.34%
(0.1,0.15)	8.0786	8.4567	95.53%

value of $\chi\%$ reflects the degree of the non-symmetry of the control loops. The larger $\chi\%$ is, the more non-symmetric the system is and the more conservatism could be introduced by symmetry-exploiting technique. Fig. 12 shows the relationship between ρ_c and $\chi\%$ which confirms our qualitative analysis. It is shown ρ_c increases quite slow as $\chi\%$ increases and ρ_c is less than 12% even when system parameters T_g, T_t and R are subject to maximal deviation of 50% of related typical values. In other words, the symmetry-exploiting is quite robust to the non-symmetry originated from parameter deviation. From our numerical experience, we found ρ_c was quite sensitive to the typical value of droop characteristics R. Fig. 13 reveals the quantitative relationship between ρ_c and typical value of R. It is observed that the smaller the typical value of R is, the more conservatism will be introduced by the structure-exploiting techniques. In fact, the smaller R is, the stronger the connection between Δf and ΔP_{vk} is. The sparsity-exploiting technique brings more conservatism when the connection between Δf and ΔP_{vk} becomes stronger. In general, compared with its significant speed-up and scale-up effects, the proposed structure-exploiting techniques introduce reasonably acceptable degree of conservatism.

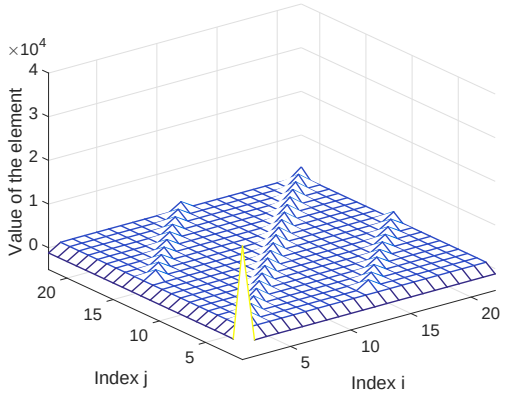

(a) Structure-exploiting DDSA

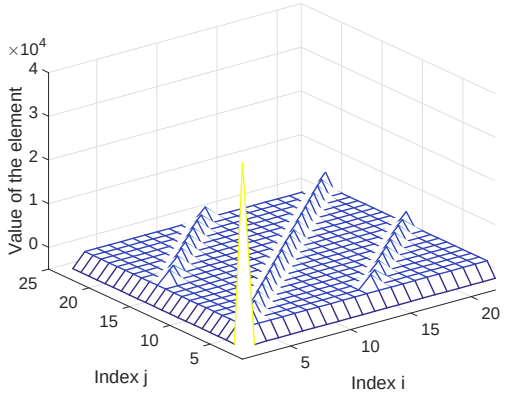

(b) Direct DDSA

Fig. 9: Comparison of mesh plots of $\boldsymbol{P}$ obtained by two methods on single-area LFC with 10 generation units

VI. Discussion

Although the main focus of this paper is stability analysis, the proposed method can also be extended to controller design. The controller should not only guarantee system stability but also provide desirable dynamic performance. In the framework of robust control, the dynamic performance is represented by some robust performance index (RPI), e.g. H_∞ norm $\sup_{\omega \neq 0} \frac{\|z\|_2}{\|\omega\|_2}$ where ω is the disturbance and z is the controlled output. In LFC, ω usually represents load disturbance and

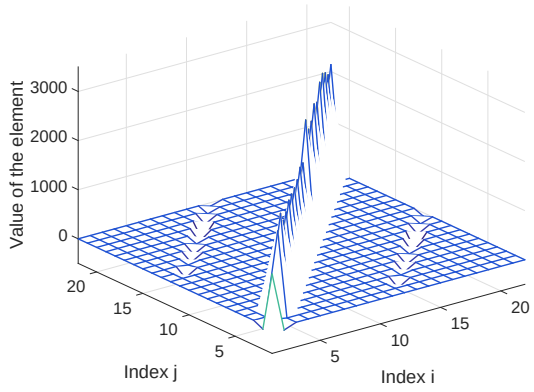

(a) Structure-exploiting DDSA

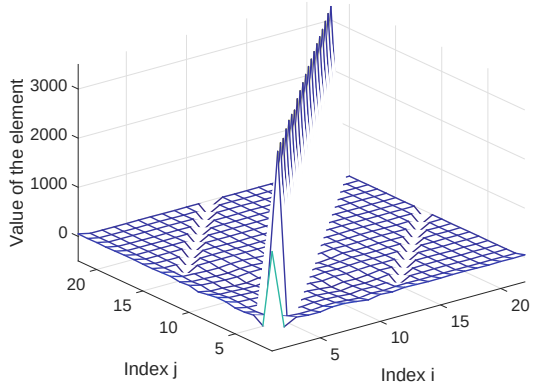

(b) Direct DDSA

Fig. 10: Comparison of mesh plots of $\boldsymbol{Q}_1$ obtained by two methods on single-area LFC with 10 generation units

z often includes frequency deviation and area control errors [15]. Every delay-dependent stability criterion can be extended to the corresponding delay-dependent BRL which provides guarantee for both system stability and dynamic performance thus can be used to design an appropriate controller. For example, the BRL corresponding to Theorem 1 is stated as follows: consider a system expressed by

$$\begin{cases} \dot{x}(t) = \boldsymbol{A}x(t) + \boldsymbol{A}_d x(t - d(t)) + \boldsymbol{B}_\omega \omega(t) \\ z(t) = \boldsymbol{C}_\omega x(t) \end{cases} \tag{19}$$

where matrix $\boldsymbol{A}_d$ is a function of the design parameter (K_P, K_I). Then the system (19) is asymptotically stable and $\sup_{\omega \neq 0} \frac{\|z\|_2}{\|\omega\|_2} < \gamma$ for any delay $0 \leq d(t) \leq \tau$ and $|\dot{d}(t)| \leq \mu$ if there exist $\boldsymbol{P} \succ \boldsymbol{0}$, $\boldsymbol{Q}_1 \succ \boldsymbol{0}$, $\boldsymbol{Q}_2 \succ \boldsymbol{0}$, $\boldsymbol{R} \succ \boldsymbol{0}$ and $\boldsymbol{S}$ such that $\boldsymbol{\Psi} \succcurlyeq \boldsymbol{0}$ and

$$\begin{bmatrix} \boldsymbol{\Phi}_{11} & \boldsymbol{\Phi}_{12} & \boldsymbol{S} & \tau \boldsymbol{A}^\top \boldsymbol{R} & \boldsymbol{P}\boldsymbol{B}_\omega & \boldsymbol{C}_\omega^T \\ \boldsymbol{\Phi}_{12}^\top & \boldsymbol{\Phi}_{22} & -\boldsymbol{S} + \boldsymbol{R} & \tau \boldsymbol{A}_d^\top \boldsymbol{R} & \boldsymbol{0} & \boldsymbol{0} \\ \boldsymbol{S}^\top & -\boldsymbol{S}^\top + \boldsymbol{R} & -\boldsymbol{R} - \boldsymbol{Q}_2 & \boldsymbol{0} & \boldsymbol{0} & \boldsymbol{0} \\ \tau \boldsymbol{R}\boldsymbol{A} & \tau \boldsymbol{R}\boldsymbol{A}_d & \boldsymbol{0} & -\boldsymbol{R} & \boldsymbol{0} & \boldsymbol{0} \\ \boldsymbol{B}_\omega^T \boldsymbol{P} & \boldsymbol{0} & \boldsymbol{0} & \boldsymbol{0} & -\gamma \boldsymbol{I}_n & \boldsymbol{0} \\ \boldsymbol{C}_\omega & \boldsymbol{0} & \boldsymbol{0} & \boldsymbol{0} & \boldsymbol{0} & -\gamma \boldsymbol{I}_n \end{bmatrix} \prec 0 \tag{20}$$

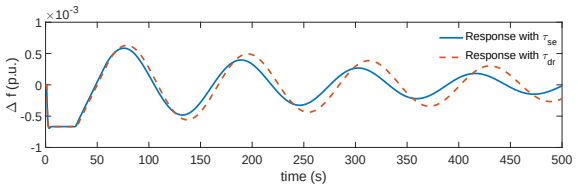

(a) $(K_P = 0.05, K_I = 0.05)$

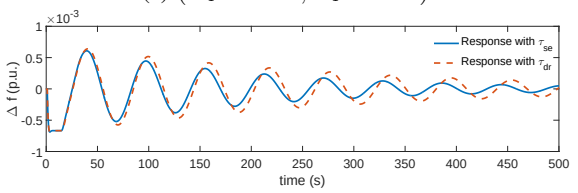

(b) $(K_P = 0.05, K_I = 0.1)$

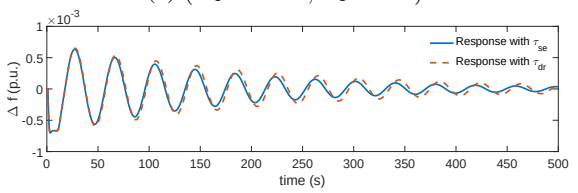

(c) $(K_P = 0.05, K_I = 0.15)$

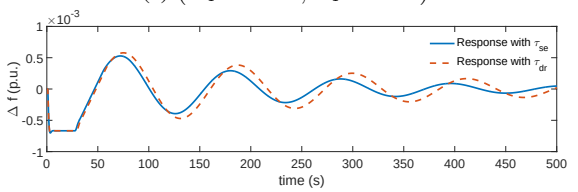

(d) $(K_P = 0.1, K_I = 0.05)$

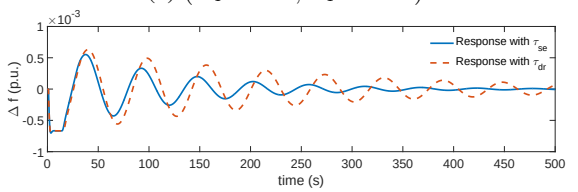

(e) $(K_P = 0.1, K_I = 0.1)$

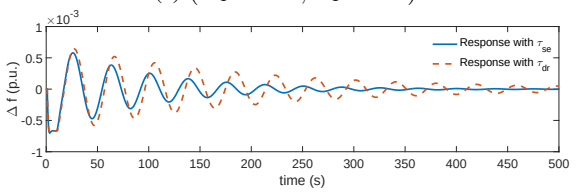

(f) $(K_P = 0.1, K_I = 0.15)$

Fig. 11: Comparison of system Frequency response of the 10-unit single-area LFC with the delay margins obtained by two methods

where $\boldsymbol{\Psi}$, $\boldsymbol{\Phi}_{11}$, $\boldsymbol{\Phi}_{12}$ and $\boldsymbol{\Phi}_{22}$ are defined as in Theorem 1. As shown above, the BRL is also a set of LMIs very similar to the stability criterion. Therefore, the sparsity and symmetry exploiting techniques proposed in this paper can be readily applied to the BRL to accelerate and scale up the control design.

More specifically, based on the framework in [31], we can design a delay-dependent H_∞ robust controller which minimizes the RPI (H_∞ norm) while maintaining stability for any delays less than a preset upper bound. By simply replacing

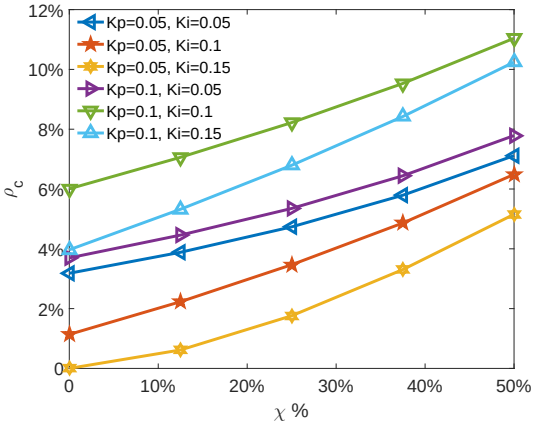

Fig. 12: Degree of additional conservatism of structure-exploiting techniques versus $\chi\%$. Typical value of R is set to be 5%.

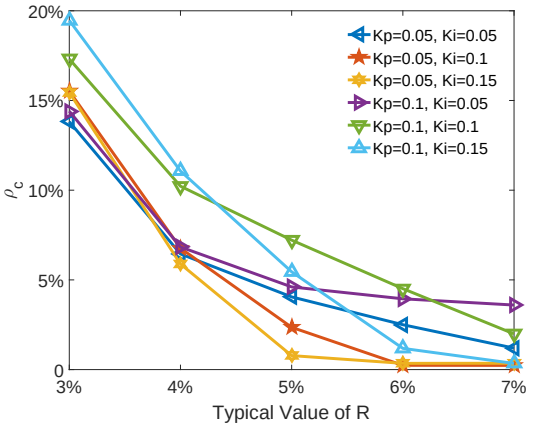

Fig. 13: Degree of additional conservatism of structure-exploiting techniques versus the typical Value of R. $\chi\%$ is set to be 25%.

Lemma 1 in [31] with the above-mentioned dealy-dependent BRL, a numerical method to design such controller is readily available. Note that the LMI needs to be solved iteratively for probably hundreds of times to converge to the optimal controller parameters; hence the accelerating and scaling-up effects provided by the proposed structure-exploiting techniques could be even more significant.

In addition, LMI-based delay-dependent stability criteria are employed to calculate the delay margins of wide-area damping controllers (WADC) installed at generator excitation systems [18] and FACTS devices [19]. Delay-dependent BRLs are also employed in [32] to design state-feedback WADC. Therefore, the structure-exploiting techniques proposed in this paper are also of potential to be applied to the analysis and synthesis of the time-delay WADC.

VII. Conclusion

In this paper, the chordal sparsity and symmetry of the graph related to time-delay LFC loops have been exploited to improve the numerical tractability of DDSA. The graph-theoretic analysis provides guidance for restricting the structure of weighting matrices in DDSA, such that the LMIs possess chordal sparsity. The symmetry of LFC loops has been utilized to reduce the number of decision variables. At the price of introducing minor conservatism, case studies show the numerical tractability and computational efficiency have been improved by orders of magnitude. Lemma 2 in this paper is a generalization of the results in [20]. Our result provides a general approach for $\boldsymbol{A}^T\boldsymbol{P}+\boldsymbol{P}\boldsymbol{A}$ to inherit the chordal sparsity of $\boldsymbol{A}$, whereas paper [20] discusses several special cases. Note that the conservatism introduced by structure-exploiting techniques are dependent on system parameters. One future direction is to derive theoretical bounds for the introduced conservatism for a certain class of systems. Another future direction is to extend the proposed method to DDSA of WADC.

Appendix A
State-space Model of Time-delayed LFC

The state-space model for the open-loop system in area i is

$$\begin{cases}\dot{x}_i(t)=\boldsymbol{A}_i x_i(t)+\sum_{j=1,j\neq i}^{N}\boldsymbol{A}_{ij}x_j(t)+\boldsymbol{B}_i u_i(t-\tau_i)\\ y_i(t)=\boldsymbol{C}_i x_i(t)\end{cases} \tag{21}$$

where

$$x_i^\top=\left[\Delta f_i,\Delta P_{tie-i},\Delta P_{m1i},\cdots,\Delta P_{mn_gi},\Delta P_{v1i},\cdots,\Delta P_{vn_gi}\right]$$

$$y_i=ACE_i$$

$$\boldsymbol{A}_i=\begin{bmatrix}\boldsymbol{A}_{11i} & \boldsymbol{A}_{12i} & \boldsymbol{0}_{2\times n_g}\\ \boldsymbol{0}_{n_g\times 2} & \boldsymbol{A}_{22i} & \boldsymbol{A}_{23i}\\ \boldsymbol{A}_{31i} & \boldsymbol{0}_{n_g\times n_g} & \boldsymbol{A}_{33i}\end{bmatrix}$$

$$\boldsymbol{A}_{ij}=\begin{bmatrix}0 & 0 & \boldsymbol{0}_{1\times 2n_g}\\ -2\pi T_{ij} & 0 & \boldsymbol{0}_{1\times 2n_g}\\ \boldsymbol{0}_{2n_g\times 1} & \boldsymbol{0}_{2n_g\times 1} & \boldsymbol{0}_{2n_g\times 2n_g}\end{bmatrix}$$

$$\boldsymbol{B}_i=\begin{bmatrix}\boldsymbol{0}_{2\times 1}\\ \boldsymbol{0}_{n_g\times 1}\\ \boldsymbol{B}_{3i}\end{bmatrix},F_i=\begin{bmatrix}\frac{-1}{M_i}\\ \boldsymbol{0}_{(1+n_g)\times 1}\\ \boldsymbol{0}_{n_g\times 1}\end{bmatrix}$$

$$\boldsymbol{C}_i=\begin{bmatrix}\beta_i & 1 & \boldsymbol{0}_{1\times 2n_g}\end{bmatrix},D_i=\begin{bmatrix}0 & -1 & \boldsymbol{0}_{1\times n_g}\end{bmatrix}$$

$$\boldsymbol{A}_{11i}=\begin{bmatrix}-\frac{D_i}{M_i} & -\frac{1}{M_i}\\ 2\pi\sum_{j=1,j\neq i}^{N}T_{ij} & 0\end{bmatrix},\boldsymbol{A}_{12i}=\begin{bmatrix}\frac{1}{M_i}&\cdots&\frac{1}{M_i}\\ 0&\cdots&0\end{bmatrix}$$

$$\boldsymbol{A}_{22i}=-\boldsymbol{A}_{23i}=diag\left\{-\tfrac{1}{T_{t1i}},\cdots,-\tfrac{1}{T_{tn_gi,}}\right\}$$

$$\boldsymbol{A}_{31i}=\begin{bmatrix}\frac{-1}{T_{g1i}R_{1i}}&\cdots&\frac{-1}{T_{gn_gi}R_{n_gi}}\\ 0&\cdots&0\end{bmatrix}^\top\boldsymbol{B}_{3i}=\begin{bmatrix}\frac{\alpha_{1i}}{T_{g1i}}&\cdots&\frac{\alpha_{n_gi}}{T_{gn_gi}}\end{bmatrix}^\top$$

$$\boldsymbol{A}_{33i}=diag\left\{\tfrac{-1}{T_{g1i}},\cdots,\tfrac{-1}{T_{gn_gi}}\right\}$$

The PI controller in area i takes the form

$$u_i(t)=-K_{Pi}ACE_i-K_{Ii}\int ACE_i dt \tag{22}$$

To simplify the analysis, further define the virtual state vectors $\bar{x}_i=[x_i^\top,\int y_i^\top]^\top$, the closed-loop system can then be rewritten as

$$\dot{\bar{x}}_i(t)=\bar{\boldsymbol{A}}_{ii}\bar{x}_i(t)+\bar{\boldsymbol{A}}_{dii}\bar{x}_i(t-\tau_i)+\sum_{j=i,j\neq i}^{N}\bar{\boldsymbol{A}}_{ij}\bar{x}_j(t) \tag{23}$$

where

$$\bar{\boldsymbol{A}}_{ii} = \begin{bmatrix} \boldsymbol{A}_i & 0 \\ \boldsymbol{C}_i & 0 \end{bmatrix},\ \bar{\boldsymbol{A}}_{dii} = \begin{bmatrix} -K_{Pi}\boldsymbol{B}_i\boldsymbol{C}_i & -K_{Ii}\boldsymbol{B}_i \\ \boldsymbol{0}_{2n_g+2} & 0 \end{bmatrix}$$
$$\bar{\boldsymbol{A}}_{ij} = \begin{bmatrix} \boldsymbol{A}_{ij} & 0 \\ 0 & 0 \end{bmatrix}$$

By defining the state vector as $x = [\bar{x}_1^\top, \bar{x}_2^\top, \cdots, \bar{x}_n^\top]^\top$, model (23) can be easily rearrange into the standard form

$$\dot{x}(t) = \boldsymbol{A}x(t) + \textstyle\sum_{i=1}^{N} \boldsymbol{A}_{di}x(t-\tau_i) \tag{24}$$

where

$$\boldsymbol{A} = \begin{bmatrix} \bar{\boldsymbol{A}}_{11} & \cdots & \bar{\boldsymbol{A}}_{1N} \\ \vdots & \ddots & \vdots \\ \bar{\boldsymbol{A}}_{N1} & \cdots & \bar{\boldsymbol{A}}_{NN} \end{bmatrix}, \boldsymbol{A}_{di} = \begin{bmatrix} \boldsymbol{0} & \cdots & \boldsymbol{0} & \cdots & \boldsymbol{0} \\ \vdots & \ddots & & & \vdots \\ \boldsymbol{0} & & \bar{\boldsymbol{A}}_{dii} & & \boldsymbol{0} \\ \vdots & & & \ddots & \vdots \\ \boldsymbol{0} & \cdots & \boldsymbol{0} & \cdots & \boldsymbol{0} \end{bmatrix}.$$

APPENDIX B
PROOFS

Proof of Lemma 2: Matrix $\boldsymbol{B}$ can be written as $\boldsymbol{B} = \sum_{(i,j)\in H} b_{ij}\boldsymbol{E}_{ij}$ where $b_{ij} \in \mathbb{R}$. Therefore it suffices to show $\boldsymbol{A}\boldsymbol{E}_{ij} \in \mathbb{M}_n(F)$ and $\boldsymbol{E}_{ij}\boldsymbol{A} \in \mathbb{M}_n(F)$, $\forall (i,j) \in H$. $\boldsymbol{A}\boldsymbol{E}_{ij}$ is obtained by putting the i^{th} column of $\boldsymbol{A}$ in the j^{th} column of a $n \times n$ zero matrix. Let G' denote the graph associated with $\boldsymbol{A}\boldsymbol{E}_{ij}$. From a graph perspective, we have

$$\begin{aligned} adj_{G'}(j) &= adj_G(i) \cup \{i\} \setminus \{j\} \\ &= (adj_G(i) \cap C_r) \cup (adj_G(i) \setminus C_r) \cup \{i\} \setminus \{j\} \\ &= (adj_G(j) \cap C_r) \cup (adj_G(j) \setminus C_r) \\ &= adj_G(j) \end{aligned} \tag{25}$$

where the first equality comes from the formation of $\boldsymbol{A}\boldsymbol{E}_{ij}$ just described and the third equality comes from the completeness of clique C_r and the defining property of $(i,j) \in H$ in (8). From (25), we conclude $\boldsymbol{A}\boldsymbol{E}_{ij} \in \mathbb{M}_n(F)$. Finally, $\boldsymbol{E}_{ij}\boldsymbol{A} \in \mathbb{M}_n(F)$ results from $\boldsymbol{A}^T\boldsymbol{E}_{ji} \in \mathbb{M}_n(F)$ noticing the undirectness of graph G. ∎

Proof of Lemma 3: Since $G^{(k)}(V^{(k)}, F^{(k)})$ is chordal, there exists a clique tree $\mathcal{T}^{(k)}(\mathcal{C}^{(k)}, \mathcal{E}^{(k)})$, $\forall k = 1, 2, \cdots, m$ according to Lemma 1, and all the clique trees can be chosen with exactly the same structure. Let $\mathcal{T}(\mathcal{C}, \mathcal{E})$ denote the tree on $\mathcal{C}$ analogous to $\mathcal{T}^{(k)}(\mathcal{C}^{(k)}, \mathcal{E}^{(k)})$. According to Lemma 1, it suffices to show $\mathcal{T}(\mathcal{C}, \mathcal{E})$ is a clique tree of graph $G(V, F)$. We first show $\mathcal{C} = \{C_1, C_2, \cdots, C_p\}$ are maximum cliques. It is explicitly shown in (10) that C_r, $\forall r = 1, \cdots, p$, is a clique of $G(V, F)$. To prove the maximality, assume $C_r' \supset C_r$ is another clique. Pick one vertex $v \in C_r' \setminus C_r$. We have $v \in V^{(k)}$ for some $k \in \{1, 2, \cdots, m\}$. Then $C_r \cap V^{(k)} \supset C_r^{(k)}$ is also a clique of $G^{(k)}(V^{(k)}, F^{(k)})$, which contradicts with the maximality of $C_r^{(k)}$. We then show the CIP holds for $\mathcal{T}(\mathcal{C}, \mathcal{E})$. For any C_i, $C_j \in \mathcal{C}$,

$$\begin{aligned} C_i \cap C_j &= \left(\cup_{k=1}^m C_i^{(k)}\right) \cap \left(\cup_{k=1}^m C_j^{(k)}\right) \\ &= \cup_{k=1}^m \left(C_i^{(k)} \cap C_j^{(k)}\right). \end{aligned} \tag{26}$$

For any C_r on the path connecting C_i and C_j, $C_r^{(k)}$ is also on the path connecting $C_r^{(i)}$ and $C_r^{(j)}$ due to the similarity of $\mathcal{T}(\mathcal{C}, \mathcal{E})$ and $\mathcal{T}^{(k)}(\mathcal{C}^{(k)}, \mathcal{E}^{(k)})$. Since $\mathcal{T}^{(k)}(\mathcal{C}^{(k)}, \mathcal{E}^{(k)})$ is a clique tree, $C_i^{(k)} \cap C_j^{(k)} \subseteq C_r^{(k)}$. Using (26), we have $C_i \cap C_j \subseteq \cup_{k=1}^m C_r^{(k)} = C_r$. Therefore, CIP holds for $\mathcal{T}(\mathcal{C}, \mathcal{E})$. We finally conclude $\mathcal{T}(\mathcal{C}, \mathcal{E})$ is a clique tree of $G(V, F)$. ∎

Proof of Lemma 4: Step 1: we show $\boldsymbol{\Phi} \in \mathbb{S}_{nm}(F^*)$, i.e. $(i,j) \in F^*$ if $[\boldsymbol{\Phi}]_{ij} \neq 0$. It suffices to consider three cases. First, note that the submatrix of $\boldsymbol{\Phi}$

$$\begin{bmatrix} \boldsymbol{\Phi}_{22} & \cdots & \boldsymbol{\Phi}_{2m} \\ \vdots & \ddots & \vdots \\ \boldsymbol{\Phi}_{m2} & \cdots & \boldsymbol{\Phi}_{mm} \end{bmatrix}$$

satisfies the conditions of Corollary 1, which implies that $\forall n+1 \leq i, j \leq nm$ with $[\boldsymbol{\Phi}]_{ij} \neq 0$, $\exists 1 \leq r \leq p$, such that $(i,j) \in (\cup_{k=1}^{m-1}(kn + C_r)) \times (\cup_{k=1}^{m-1}(kn + C_r))$, leading to $(i,j) \in C_r^* \times C_r^*$. Second, $\forall 1 \leq i \leq n < j \leq nm$ with $[\boldsymbol{\Phi}]_{ij} \neq 0$, we have $(i, j \bmod n) \in F$ according to the chordal structure of each block other than $\boldsymbol{\Phi}_{11}$. Hence $\exists 1 \leq r \leq p$, such that $(i, j \bmod n) \in C_r \times C_r$, which implies $(i,j) \in C_r^* \times C_r^*$ by definition. Third, $\forall 1 \leq i, j \leq n$, it is obvious that $(i,j) \in C_0^* \times C_0^*$.

Step 2: we prove $G^*(V^*, F^*)$ is chordal by showing the maximality of cliques $\mathcal{C}^* = \{C_0^*, C_1^*, \cdots, C_p^*\}$ and the existence of a clique tree $\mathcal{T}^*(\mathcal{C}^*, \mathcal{E}^*)$. First, the maximality of cliques $\mathcal{C}^*$ relies on the observation that $C_r^* \nsubseteq C_t^*$, $\forall\ 0 \leq r, t \leq p$ by definition. Second, we define $\mathcal{T}^*(\mathcal{C}^*, \mathcal{E}^*)$ a tree on $\mathcal{C}^*$ as depicted in Fig. 14. To check CIP holds for $\mathcal{T}^*(\mathcal{C}^*, \mathcal{E}^*)$,

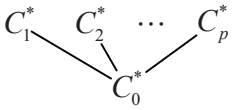

Fig. 14: Clique Tree of Chordal Graph $G^*(V^*, F^*)$

it suffices to show $C_r^* \cap C_t^* \subseteq C_0^*$, $\forall\ 1 \leq r < t \leq p$. Note that

$$\begin{aligned} C_r^* \cap C_t^* &= \left(\cup_{k=0}^{m-1}(kn + C_r)\right) \cap \left(\cup_{k=0}^{m-1}(kn + C_t)\right) \\ &= \cup_{k=0}^{m-1}\left(kn + C_r \cap C_t\right) \\ &\subseteq \cup_{k=0}^{m-1}\left(kn + \hat{V}\right) \\ &\subseteq C_0^*. \end{aligned} \tag{27}$$

The two inclusions in (27) come from the definitions of $\hat{V}$ and C_0^*, respectively. Therefore, $\mathcal{T}^*(\mathcal{C}^*, \mathcal{E}^*)$ is a clique tree. Using Lemma 1, we conclude $G^*(V^*, F^*)$ is chordal.

Step 1 and step 2 together lead to the lemma. ∎

REFERENCES

[1] X. Yu and K. Tomsovic, "Application of linear matrix inequalities for load frequency control with communication delays," *IEEE Trans. Power Syst.*, vol. 19, no. 3, pp. 1508–1515, 2004.

[2] L. Jiang, W. Yao, Q. Wu, J. Wen, and S. Cheng, "Delay-dependent stability for load frequency control with constant and time-varying delays," *IEEE Trans. Power Syst.*, vol. 27, no. 2, pp. 932–941, 2012.

[3] C.-K. Zhang, L. Jiang, Q. Wu, Y. He, and M. Wu, "Delay-dependent robust load frequency control for time delay power systems," *IEEE Trans. Power Syst.*, vol. 28, no. 3, pp. 2192–2201, 2013.

[4] C.-K. Zhang, L. Jiang, Q. Wu, Y. He, and M. Wu, "Further results on delay-dependent stability of multi-area load frequency control," *IEEE Trans. Power Syst.*, vol. 28, no. 4, pp. 4465–4474, 2013.

[5] S. Snmez, S. Ayasun, and C. O. Nwankpa, "An exact method for computing delay margin for stability of load frequency control systems with constant communication delays," *IEEE Trans. Power Syst.*, vol. 31, pp. 370–377, Jan 2016.

[6] W. Michiels and S.-I. Niculescu, *Stability, Control, and Computation for Time-Delay Systems: An Eigenvalue-Based Approach*, vol. 27. SIAM, 2014.

[7] F. Milano, "Small-signal stability analysis of large power systems with inclusion of multiple delays," *IEEE Trans. Power Syst.*, vol. 31, pp. 3257–3266, July 2016.

[8] H. Jia and X. Yu, "A simple method for power system stability analysis with multiple time delays," in *Power and Energy Society General Meeting-Conversion and Delivery of Electrical Energy in the 21st Century, 2008 IEEE*, pp. 1–7, IEEE, 2008.

[9] S. Ayasun, U. Eminoğlu, and Ş. Sönmez, "Computation of stability delay margin of time-delayed generator excitation control system with a stabilizing transformer," *Mathematical Problems in Engineering*, vol. 2014, 2014.

[10] S. Sönmez, S. Ayasun, and U. Eminoglu, "Computation of time delay margins for stability of a single-area load frequency control system with communication delays," *WSEAS Trans. Power Syst*, vol. 9, pp. 67–76, 2014.

[11] S. Sönmez and S. Ayasun, "Stability region in the parameter space of pi controller for a single-area load frequency control system with time delay," *IEEE Trans. Power Syst.*, vol. 31, no. 1, pp. 829–830, 2016.

[12] J. M. Thangaiah and R. Parthasarathy, "Delay-dependent stability analysis of power system considering communication delays," *International Transactions on Electrical Energy Systems*, 2016.

[13] M. Wu, Y. He, and J.-H. She, *Stability analysis and robust control of time-delay systems*. Springer, 2010.

[14] K. Ramakrishnan and G. Ray, "Stability criteria for nonlinearly perturbed load frequency systems with time-delay," *IEEE Journal on Emerging and Selected Topics in Circuits and Systems*, vol. 5, no. 3, pp. 383–392, 2015.

[15] H. Bevrani, *Robust power system frequency control*, vol. 85. Springer, 2009.

[16] A. Ahmadi and M. Aldeen, "An lmi approach to the design of robust delay-dependent overlapping load frequency control of uncertain power systems," *International Journal of Electrical Power & Energy Systems*, vol. 81, pp. 48–63, 2016.

[17] C. Peng and J. Zhang, "Delay-distribution-dependent load frequency control of power systems with probabilistic interval delays," *IEEE Trans. Power Syst.*, vol. 31, no. 4, pp. 3309–3317, 2016.

[18] W. Yao, L. Jiang, Q. Wu, J. Wen, and S. Cheng, "Delay-dependent stability analysis of the power system with a wide-area damping controller embedded," *IEEE Trans. Power Syst.*, vol. 26, no. 1, pp. 233–240, 2011.

[19] W. Yao, L. Jiang, J. Wen, Q. Wu, and S. Cheng, "Wide-area damping controller of facts devices for inter-area oscillations considering communication time delays," *IEEE Trans. Power Syst.*, vol. 29, no. 1, pp. 318–329, 2014.

[20] R. P. Mason and A. Papachristodoulou, "Chordal sparsity, decomposing sdps and the lyapunov equation," in *American Control Conference (ACC), 2014*, pp. 531–537, IEEE, 2014.

[21] P. Kundur, N. J. Balu, and M. G. Lauby, *Power system stability and control*, vol. 7. McGraw-hill New York, 1994.

[22] P. Park, J. W. Ko, and C. Jeong, "Reciprocally convex approach to stability of systems with time-varying delays," *Automatica*, vol. 47, no. 1, pp. 235–238, 2011.

[23] J. R. Blair and B. Peyton, "An introduction to chordal graphs and clique trees," in *Graph theory and sparse matrix computation*, pp. 1–29, Springer, 1993.

[24] S. Kim, M. Kojima, M. Mevissen, and M. Yamashita, "Exploiting sparsity in linear and nonlinear matrix inequalities via positive semidefinite matrix completion," *Mathematical programming*, vol. 129, no. 1, pp. 33–68, 2011.

[25] M. Artin, *Algebra*. Prentice Hall, 1991.

[26] J. Löfberg, "Yalmip: A toolbox for modeling and optimization in matlab," in *Computer Aided Control Systems Design, 2004 IEEE International Symposium on*, pp. 284–289, IEEE, 2004.

[27] R. H. Tütüncü, K. C. Toh, and M. J. Todd, "Solving semidefinite-quadratic-linear programs using sdpt3," *Mathematical programming*, vol. 95, no. 2, pp. 189–217, 2003.

[28] T. Athay, R. Podmore, and S. Virmani, "A practical method for the direct analysis of transient stability," *IEEE Transactions on Power Apparatus and Systems*, no. 2, pp. 573–584, 1979.

[29] R. D. Zimmerman, C. E. Murillo-Sánchez, and R. J. Thomas, "Matpower: Steady-state operations, planning, and analysis tools for power systems research and education," *IEEE Trans. Power Syst.*, vol. 26, no. 1, pp. 12–19, 2011.

[30] K. Nakata, K. Fujisawa, M. Fukuda, M. Kojima, and K. Murota, "Exploiting sparsity in semidefinite programming via matrix completion ii: Implementation and numerical results," *Mathematical Programming*, vol. 95, no. 2, pp. 303–327, 2003.

[31] D. Rerkpreedapong, A. Hasanovic, and A. Feliachi, "Robust load frequency control using genetic algorithms and linear matrix inequalities," *IEEE Trans. Power Syst.*, vol. 18, no. 2, pp. 855–861, 2003.

[32] J. Li, Z. Chen, D. Cai, W. Zhen, and Q. Huang, "Delay-dependent stability control for power system with multiple time-delays," *IEEE Trans. Power Syst.*, vol. 31, pp. 2316–2326, May 2016.

Chao Duan (S'14) was born in Chongqing, China, in 1989. He received the B.S. degree in electrical engineering from Xi'an Jiaotong University, Xi'an, China, in 2012. He is currently pursuing the Ph.D. degree at Xi'an Jiaotong University, Xi'an, China, and the University of Liverpool, Liverpool, U.K.

His research interests are in stochastic optimization, stability analysis and robust control of power systems.

Chuan-Ke Zhang (S'12) received the B.Sc. degree in automation and the Ph.D. degree in control science and engineering from Central South University, Changsha, China, in 2007 and 2013, respectively.

He was a Research Assistant and a Post-Doctoral Research Associate with the Department of Electrical Engineering and Electronics, University of Liverpool, Liverpool, U.K., from 2011 to 2013, and form 2014 to 2016, respectively. He joined the School of Automation, China University of Geosciences, Wuhan, China, in 2014. He is currently an Associate Professor with the School of Automation, China University of Geosciences. His current research interests include time-delay systems, chaos synchronization, and power system stability and control.

Lin Jiang (M'00) received the B.Sc. and M.Sc. degrees from Huazhong University of Science and Technology (HUST), China, in 1992 and 1996; and the Ph.D. degree from the University of Liverpool, UK, in 2001, all in Electrical Engineering.

He worked as a Postdoctoral Research Assistant in the University of Liverpool from 2001 to 2003, and Postdoctoral Research Associate in the Department of Automatic Control and Systems Engineering, the University of Sheffield from 2003 to 2005. He was a Senior Lecturer at the University of Glamorgam from 2005 to 2007 and moved to the University of Liverpool in 2007. Currently, he is a Reader in The University of Liverpool. His current research interests include control and analysis of power system, smart grid, and renewable energy.

Wanliang Fang was born in Henan, China, in 1958. He received the B.S. and M.S. degrees from Xi'an Jiaotong University, Xi'an, China in 1982 and 1988, respectively, and the Ph.D. degree from Hong Kong Polytechnic University, HongKong, in 1999, all in electrical engineering.

He is currently a Professor of electrical engineering at Xi'an Jiaotong University. His research interests include power system stability analysis and control, FACTS and HVDC.

Wei Yao (M'13) received the B.Sc. and Ph.D. degrees in electrical engineering from the Huazhong University of Science and Technology (HUST), Wuhan, China, in 2004 and 2010, respectively.

He was a Post-Doctoral Researcher with the Department of Power Engineering, HUST, from 2010 to 2012, where he is currently an associate professor with the School of Electrical and Electronics Engineering. Since 2012, he has been a Post-Doctoral Research Associate with the Department of Electrical Engineering and Electronics, University of Liverpool, Liverpool, U.K. His current research interests include power system stability analysis and control, and renewable energy.